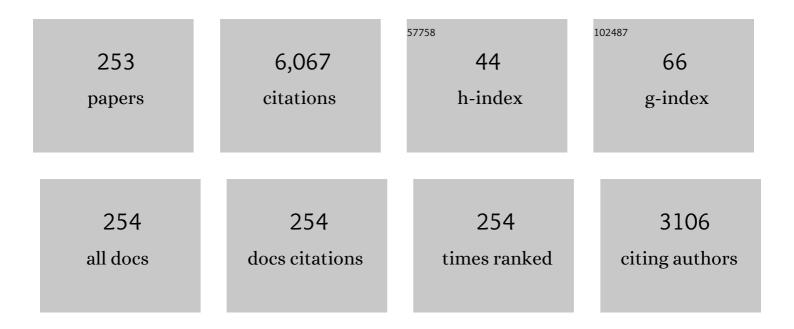
Xiaofeng Li

List of Publications by Year in descending order

Source: https://exaly.com/author-pdf/975528/publications.pdf Version: 2024-02-01



#	Article	IF	CITATIONS
1	Sea Surface Wind Speed Retrieval From Textures in Synthetic Aperture Radar Imagery. IEEE Transactions on Geoscience and Remote Sensing, 2022, 60, 1-11.	6.3	4
2	A Deep Learning Model to Extract Ship Size From Sentinel-1 SAR Images. IEEE Transactions on Geoscience and Remote Sensing, 2022, 60, 1-14.	6.3	15
3	Tropical Cyclone Intensity Estimation From Geostationary Satellite Imagery Using Deep Convolutional Neural Networks. IEEE Transactions on Geoscience and Remote Sensing, 2022, 60, 1-16.	6.3	22
4	An Automatic Algorithm for Estimating Tropical Cyclone Centers in Synthetic Aperture Radar Imagery. IEEE Transactions on Geoscience and Remote Sensing, 2022, 60, 1-16.	6.3	1
5	Underwater Image Enhancement via Physical-Feedback Adversarial Transfer Learning. IEEE Journal of Oceanic Engineering, 2022, 47, 76-87.	3.8	25
6	Development of a Dual-Attention U-Net Model for Sea Ice and Open Water Classification on SAR Images. IEEE Geoscience and Remote Sensing Letters, 2022, 19, 1-5.	3.1	45
7	Tropical Cyclone Center and Symmetric Structure Estimating From SMAP Data. IEEE Transactions on Geoscience and Remote Sensing, 2022, 60, 1-11.	6.3	4
8	Development of a component-based interactive visualization system for the analysis of ocean data. Big Earth Data, 2022, 6, 219-235.	4.4	4
9	Multilayer Fusion Recurrent Neural Network for Sea Surface Height Anomaly Field Prediction. IEEE Transactions on Geoscience and Remote Sensing, 2022, 60, 1-11.	6.3	3
10	Automatic Waterline Extraction and Topographic Mapping of Tidal Flats From SAR Images Based on Deep Learning. Geophysical Research Letters, 2022, 49, .	4.0	23
11	Oceanic internal wave amplitude retrieval from satellite images based on a data-driven transfer learning model. Remote Sensing of Environment, 2022, 272, 112940.	11.0	28
12	AlgaeNet: A Deep-Learning Framework to Detect Floating Green Algae From Optical and SAR Imagery. IEEE Journal of Selected Topics in Applied Earth Observations and Remote Sensing, 2022, 15, 2782-2796.	4.9	19
13	Physics-informed deep-learning parameterization of ocean vertical mixing improves climate simulations. National Science Review, 2022, 9, .	9.5	29
14	The Fusion of Physical, Textural, and Morphological Information in SAR Imagery for Hurricane Wind Speed Retrieval Based on Deep Learning. IEEE Transactions on Geoscience and Remote Sensing, 2022, 60, 1-13.	6.3	4
15	A Data-Driven Deep Learning Model for Weekly Sea Ice Concentration Prediction of the Pan-Arctic During the Melting Season. IEEE Transactions on Geoscience and Remote Sensing, 2022, 60, 1-19.	6.3	12
16	Classifying Sea Ice Types with a U-Net Model from Dual-polarized Sentinel-1 Images and GLCM Texture Feature. , 2022, , .		1
17	Automatic Waterline Extraction of Tidal Flats from SAR Images Based on Deep Convolutional Neural Networks. , 2022, , .		1
18	A Machine-learning-based Model to Inverse Internal Solitary Wave Amplitude from Satellite Image. , 2022, , .		0

#	Article	IF	CITATIONS
19	A Deep Learning-based Model for Cold Anticyclonic Eddies and Warm Cyclonic Eddies Detection in the Kuroshio Extension. , 2022, , .		0
20	Carbon Sinks and Variations of <i>p</i> CO ₂ in the Southern Ocean From 1998 to 2018 Based on a Deep Learning Approach. IEEE Journal of Selected Topics in Applied Earth Observations and Remote Sensing, 2021, 14, 3495-3503.	4.9	14
21	Dynamical Ocean Responses to Typhoon Malakas (2016) in the Vicinity of Taiwan. Journal of Geophysical Research: Oceans, 2021, 126, e2020JC016663.	2.6	12
22	Combination of Satellite Observations and Machine Learning Method for Internal Wave Forecast in the Sulu and Celebes Seas. IEEE Transactions on Geoscience and Remote Sensing, 2021, 59, 2822-2832.	6.3	31
23	Effects of Temperature on Sea Surface Radar Backscattering Under Neutral and Nonneutral Atmospheric Conditions for Wind Retrieval Applications: A Numerical Study. IEEE Transactions on Geoscience and Remote Sensing, 2021, 59, 2727-2743.	6.3	7
24	Microwave Satellite Measurements for Coastal Area and Extreme Weather Monitoring. Remote Sensing, 2021, 13, 3126.	4.0	9
25	Characteristics of Global Ocean Abnormal Mesoscale Eddies Derived From the Fusion of Sea Surface Height and Temperature Data by Deep Learning. Geophysical Research Letters, 2021, 48, e2021GL094772.	4.0	34
26	Developing big ocean system in support of Sustainable Development Goals: challenges and countermeasures. Big Earth Data, 2021, 5, 557-575.	4.4	8
27	A Machine-Learning Model for Forecasting Internal Wave Propagation in the Andaman Sea. IEEE Journal of Selected Topics in Applied Earth Observations and Remote Sensing, 2021, 14, 3095-3106.	4.9	22
28	A Deep Learning Model for Eddy Tracking Based on Multi-Source Remote Sensing Imagery. , 2021, , .		0
29	Classification of Multi-Channel SAR Data Based on MB-U ² -ACNet Model for Shanghai Nanhui Dongtan Intertidal Zone Environment Monitoring. , 2021, , .		2
30	The Retrieval of Hurricane Wind Speed Based on the Support Vector Machine. , 2021, , .		1
31	Satellite-Data-Driven Propagation Speed Model for Internal Solitary Waves in the Shallow and Deep Oceans. , 2021, , .		1
32	A Deep Learning Model for Subsurface Mesoscale Eddy Detection Based on Remote Sensing Images. , 2021, , .		0
33	Predicting Daily Arctic Sea Ice Concentration in the Melt Season Based on a Deep Fully Convolution Network Model. , 2021, , .		0
34	Quantitative Evaluation of Algae Detection Based on Deep Neural Network Multi-Source Data Fusion. , 2021, , .		0
35	Distribution Characteristics of Green Algae in Yellow Sea Using an Deep Learning Automatic Detection Procedure. , 2021, , .		6
36	Classifying Sea Ice Types from SAR Images Using a U-Net-Based Deep Learning Model. , 2021, , .		2

#	Article	IF	CITATIONS
37	Tropical Cyclone Winds and Inflow Angle Asymmetry From SAR Imagery. Geophysical Research Letters, 2021, 48, e2021GL095699.	4.0	7
38	Sea-land Segmentation of Synthetic Aperture Radar Imagery Using Deep Neural Network Models. , 2021, , .		0
39	Purely satellite data–driven deep learning forecast of complicated tropical instability waves. Science Advances, 2020, 6, eaba1482.	10.3	122
40	Improving seismic remote sensing of typhoon with a three-dimensional Earth model. Journal of the Acoustical Society of America, 2020, 148, 478-491.	1.1	2
41	Characteristics and generations of internal wave in the Sulu Sea inferred from optical satellite images. Journal of Oceanology and Limnology, 2020, 38, 1435-1444.	1.3	19
42	Deep-learning-based information mining from ocean remote-sensing imagery. National Science Review, 2020, 7, 1584-1605.	9.5	197
43	A Novel Marine Oil Spillage Identification Scheme Based on Convolution Neural Network Feature Extraction From Fully Polarimetric SAR Imagery. IEEE Access, 2020, 8, 59801-59820.	4.2	35
44	A Deep Learning Model for Oceanic Mesoscale Eddy Detection Based on Multi-source Remote Sensing Imagery. , 2020, , .		2
45	Automatic Extraction of Internal Wave Signature from Multiple Satellite Sensors Based on Deep Convolutional Neural Networks. , 2020, , .		3
46	Automatic Mapping of Tropical Cyclone-Induced Coastal Inundation in SAR Imagery Based on Clustering of Deep Features. , 2020, , .		1
47	A Numerical Study of SST Effects on Ocean Radar Backscattering. , 2020, , .		1
48	Sea Ice and Open Water Classification of SAR Images Using a Deep Learning Model. , 2020, , .		6
49	CNN-Based Tropical Cyclone Track Forecasting from Satellite Infrared Images. , 2020, , .		1
50	Satellite Observation of Tansmeridional Propagating Internal Waves in the Celebes Sea. , 2020, , .		2
51	Using Artificial Neural Network Ensembles With Crogging Resampling Technique to Retrieve Sea Surface Temperature From HY-2A Scanning Microwave Radiometer Data. IEEE Transactions on Geoscience and Remote Sensing, 2019, 57, 985-1000.	6.3	10
52	Wave parameters retrieval for dual-polarization C-band synthetic aperture radar using a theoretical-based algorithm under cyclonic conditions. Acta Oceanologica Sinica, 2019, 38, 21-31.	1.0	14
53	Automatically Locate Tropical Cyclone Centers Using Top Cloud Motion Data Derived From Geostationary Satellite Images. IEEE Transactions on Geoscience and Remote Sensing, 2019, 57, 10175-10190.	6.3	16
54	Sea State Bias Variability in Satellite Altimetry Data. Remote Sensing, 2019, 11, 1176.	4.0	7

#	Article	IF	CITATIONS
55	A Novel Vessel Velocity Estimation Method Using Dual-Platform TerraSAR-X and TanDEM-X Full Polarimetric SAR Data in Pursuit Monostatic Mode. IEEE Transactions on Geoscience and Remote Sensing, 2019, 57, 6130-6144.	6.3	9
56	Self-Paced Convolutional Neural Network for PolSAR Images Classification. Remote Sensing, 2019, 11, 424.	4.0	7
57	Estimating Typhoon Intensity with Convolutional Neural Network. , 2019, , .		4
58	Coastal Inundation Mapping From Bitemporal and Dualâ€Polarization SAR Imagery Based on Deep Convolutional Neural Networks. Journal of Geophysical Research: Oceans, 2019, 124, 9101-9113.	2.6	51
59	The impact of rain to observed signal from Chinese Gaofen-3 synthetic aperture radar in typhoons. Acta Oceanologica Sinica, 2019, 38, 121-133.	1.0	17
60	Sea Surface Wind Retrieval from Synthetic Aperture Radar Data by Deep Convolutional Neural Networks. , 2019, , .		5
61	Retrieval of Winds and Waves from Synthetic Aperture Radar Imagery. , 2019, , 285-303.		2
62	Ship Detection From PolSAR Imagery Using the Complete Polarimetric Covariance Difference Matrix. IEEE Transactions on Geoscience and Remote Sensing, 2019, 57, 2824-2839.	6.3	49
63	Identification of Tropical Cyclone Centers in SAR Imagery Based on Template Matching and Particle Swarm Optimization Algorithms. IEEE Transactions on Geoscience and Remote Sensing, 2019, 57, 598-608.	6.3	19
64	Activities of the GRSS Washington/Northern Virginia Chapter [Chapters]. IEEE Geoscience and Remote Sensing Magazine, 2018, 6, 47-48.	9.6	0
65	Tropical Cyclone Boundary Layer Rolls in Synthetic Aperture Radar Imagery. Journal of Geophysical Research: Oceans, 2018, 123, 2981-2996.	2.6	20
66	Sea Surface Temperature Retrieval from the First Korean Geostationary Satellite COMS Data: Validation and Error Assessment. Remote Sensing, 2018, 10, 1916.	4.0	21
67	Analysis of impacting factors on polarimetric SAR oil spill detection. Acta Oceanologica Sinica, 2018, 37, 77-87.	1.0	3
68	Classification of PolSAR Images Using Multilayer Autoencoders and a Self-Paced Learning Approach. Remote Sensing, 2018, 10, 110.	4.0	30
69	Upper Ocean Response to Typhoon Kalmaegi and Sarika in the South China Sea from Multiple-Satellite Observations and Numerical Simulations. Remote Sensing, 2018, 10, 348.	4.0	47
70	Seismological Observations of Ocean Swells Induced by Typhoon Megi Using Dispersive Microseisms Recorded in Coastal Areas. Remote Sensing, 2018, 10, 1437.	4.0	7
71	Seismic Remote Sensing of Super Typhoon Lupit (2009) with Seismological Array Observation in NE China. Remote Sensing, 2018, 10, 235.	4.0	8
72	Spatio-Temporal Variability of Annual Sea Level Cycle in the Baltic Sea. Remote Sensing, 2018, 10, 528.	4.0	5

#	Article	IF	CITATIONS
73	Development of a Gray-Level Co-Occurrence Matrix-Based Texture Orientation Estimation Method and Its Application in Sea Surface Wind Direction Retrieval From SAR Imagery. IEEE Transactions on Geoscience and Remote Sensing, 2018, 56, 5244-5260.	6.3	45
74	A C-Band Geophysical Model Function for Determining Coastal Wind Speed Using Synthetic Aperture Radar. IEEE Journal of Selected Topics in Applied Earth Observations and Remote Sensing, 2018, 11, 2417-2428.	4.9	55
75	Impact of Ships and Ocean Fronts on Coastal Sea Surface Wind Measurements From the Advanced Scatterometer. IEEE Journal of Selected Topics in Applied Earth Observations and Remote Sensing, 2018, 11, 2162-2169.	4.9	18
76	Retrieving Hurricane Wind Speed From Dominant Wave Parameters. IEEE Journal of Selected Topics in Applied Earth Observations and Remote Sensing, 2017, 10, 2589-2598.	4.9	15
77	Estuarine Plume: A Case Study by Satellite SAR Observations and <italic>In Situ</italic> Measurements. IEEE Transactions on Geoscience and Remote Sensing, 2017, 55, 2276-2287.	6.3	7
78	Observation of Wind Direction Change on the Sea Surface Temperature Front Using High-Resolution Full Polarimetric SAR Data. IEEE Journal of Selected Topics in Applied Earth Observations and Remote Sensing, 2017, 10, 2599-2607.	4.9	22
79	Impacts of oil spills on altimeter waveforms and radar backscatter cross section. Journal of Geophysical Research: Oceans, 2017, 122, 3621-3637.	2.6	13
80	Remote Sensing Studies of Suspended Sediment Concentration Variations in a Coastal Bay During the Passages of Atmospheric Cold Fronts. IEEE Journal of Selected Topics in Applied Earth Observations and Remote Sensing, 2017, 10, 2608-2622.	4.9	10
81	Observing Typhoons from Satellite-Derived Images. Springer Natural Hazards, 2017, , 183-214.	0.3	0
82	Coupled Nature of Hurricane Wind and Wave Properties for Ocean Remote Sensing of Hurricane Wind Speed. Springer Natural Hazards, 2017, , 215-236.	0.3	1
83	Synthetic Aperture Radar Observations of Extreme Hurricane Wind and Rain. Springer Natural Hazards, 2017, , 299-346.	0.3	0
84	Tropical Cyclone Multiscale Wind Features from Spaceborne Synthetic Aperture Radar. Springer Natural Hazards, 2017, , 25-39.	0.3	3
85	Tropical Cyclone Wind Field Reconstruction from SAR and Analytical Model. Springer Natural Hazards, 2017, , 69-84.	0.3	0
86	A Hurricane Wind Speed Retrieval Model for C-Band RADARSAT-2 Cross-Polarization ScanSAR Images. IEEE Transactions on Geoscience and Remote Sensing, 2017, 55, 4766-4774.	6.3	87
87	Compact Polarimetric Synthetic Aperture Radar for Marine Oil Platform and Slick Detection. IEEE Transactions on Geoscience and Remote Sensing, 2017, 55, 1407-1423.	6.3	30
88	A Hurricane Morphology and Sea Surface Wind Vector Estimation Model Based on C-Band Cross-Polarization SAR Imagery. IEEE Transactions on Geoscience and Remote Sensing, 2017, 55, 1743-1751.	6.3	50
89	A Fully Polarimetric SAR Imagery Classification Scheme for Mud and Sand Flats in Intertidal Zones. IEEE Transactions on Geoscience and Remote Sensing, 2017, 55, 1734-1742.	6.3	33
90	Internal Solitary Wave Reflection Near Dongsha Atoll, the South China Sea. Journal of Geophysical Research: Oceans, 2017, 122, 7978-7991.	2.6	40

#	Article	IF	CITATIONS
91	Bridging the gap between cyclone wind and wave by <scp>C</scp> â€band <scp>SAR</scp> measurements. Journal of Geophysical Research: Oceans, 2017, 122, 6714-6724.	2.6	41
92	Development and validation of an ocean wave retrieval algorithm for VV-polarization Sentinel-1 SAR data. Acta Oceanologica Sinica, 2017, 36, 95-101.	1.0	31
93	A Salient Region Detection and Pattern Matching-Based Algorithm for Center Detection of a Partially Covered Tropical Cyclone in a SAR Image. IEEE Transactions on Geoscience and Remote Sensing, 2017, 55, 280-291.	6.3	35
94	Ocean Upwelling Along the Yellow Sea Coast of China Revealed by Satellite Observations and Numerical Simulation. IEEE Transactions on Geoscience and Remote Sensing, 2017, 55, 526-536.	6.3	14
95	Sea Fetch Observed by Synthetic Aperture Radar. IEEE Transactions on Geoscience and Remote Sensing, 2017, 55, 272-279.	6.3	8
96	Application sentinel-1 SAR data for ocean research and operation. , 2017, , .		0
97	A weighted joint sparse of three channels method for full POL-SAR data classification. , 2017, , .		2
98	From research to operations based on contributions from Werner Alpers. , 2017, , .		1
99	The impact of oceanographic conditions on fishing ground distribution of flying squid (Ommastrephes bartrami) in the Western North Pacific using remotely sensed satellite data. , 2017, , .		1
100	Geostationary satellite observations and numerical simulation of typhoon-induced upwelling to the Northeast of Taiwan. , 2017, , .		4
101	An Empirical Algorithm for Wave Retrieval from Co-Polarization X-Band SAR Imagery. Remote Sensing, 2017, 9, 711.	4.0	14
102	Estimating Tropical Cyclone Size in the Northwestern Pacific from Geostationary Satellite Infrared Images. Remote Sensing, 2017, 9, 728.	4.0	34
103	Ocean Oil Spill Classification with RADARSAT-2 SAR Based on an Optimized Wavelet Neural Network. Remote Sensing, 2017, 9, 799.	4.0	45
104	Technical Evaluation of Sentinel-1 IW Mode Cross-Pol Radar Backscattering from the Ocean Surface in Moderate Wind Condition. Remote Sensing, 2017, 9, 854.	4.0	27
105	Mechanisms of SAR Imaging of Shallow Water Topography of the Subei Bank. Remote Sensing, 2017, 9, 1203.	4.0	13
106	SAR imaging of internal gravity waves: From atmosphere to ocean. , 2017, , .		0
107	SAR imaging of oceanic and atmospheric gravity waves. , 2017, , .		0

5

#	Article	IF	CITATIONS
109	An Improved Local Gradient Method for Sea Surface Wind Direction Retrieval from SAR Imagery. Remote Sensing, 2017, 9, 671.	4.0	34
110	Extracting Hurricane Eye Morphology from Spaceborne SAR Images Using Morphological Analysis. Springer Natural Hazards, 2017, , 119-139.	0.3	2
111	Tropical Cyclone Center Location in SAR Images Based on Feature Learning and Visual Saliency. Springer Natural Hazards, 2017, , 141-181.	0.3	3
112	Electromagnetic Scattering of Rainfall and Tropical Cyclones over Ocean. Springer Natural Hazards, 2017, , 271-298.	0.3	1
113	Tropical Cyclone Eye Morphology and Extratropical-Cyclone-Forced Mountain Lee Waves on SAR Imagery. Springer Natural Hazards, 2017, , 373-398.	0.3	0
114	Variability of Atmospheric, Oceanic, and Hydrological Phenomena. Advances in Meteorology, 2016, 2016, 1-1.	1.6	0
115	Ocean Wave Parameters Retrieval from Sentinel-1 SAR Imagery. Remote Sensing, 2016, 8, 707.	4.0	54
116	Polarimetric Analysis of Compact-Polarimetry SAR Architectures for Sea Oil Slick Observation. IEEE Transactions on Geoscience and Remote Sensing, 2016, 54, 5862-5874.	6.3	60
117	Rain effects on the hurricane observations over the ocean by Câ€band Synthetic Aperture Radar. Journal of Geophysical Research: Oceans, 2016, 121, 14-26.	2.6	43
118	SAR imaging and numerical simulation of upwelling processes near the coastal area of Qingdao in China. , 2016, , .		1
119	Application Sentinel-1 SAR data for ocean research and operation. , 2016, , .		1
120	Foreword to the Special Issue on the Remote Sensing of the World Oceans. IEEE Journal of Selected Topics in Applied Earth Observations and Remote Sensing, 2016, 9, 4895-4897.	4.9	0
121	Marine oil slick and platform detection by compact polrimetric synthetic aperture radar. , 2016, , .		2
122	SAR observation and WRF model simulation of land breeze in Hainan Island, China. , 2016, , .		0
123	SAR Observation of Eddy-Induced Mode-2 Internal Solitary Waves in the South China Sea. IEEE Transactions on Geoscience and Remote Sensing, 2016, 54, 6674-6686.	6.3	35
124	Coastal Zone Classification With Fully Polarimetric SAR Imagery. IEEE Geoscience and Remote Sensing Letters, 2016, 13, 1616-1620.	3.1	25
125	Remote sensing observations and numerical studies of a super typhoon-induced suspended sediment concentration variation in the East China Sea. Ocean Modelling, 2016, 104, 187-202.	2.4	26
126	Dynamical analysis of a satelliteâ€observed anticyclonic eddy in the northern Bering Sea. Journal of Geophysical Research: Oceans, 2016, 121, 3517-3531.	2.6	8

					1
- Y	1 / /		ΕN	C	
\sim	IAV	JF	EIN	U I	

#	Article	IF	CITATIONS
127	SAR Observation and Numerical Simulation of Mountain Lee Waves Near Kuril Islands Forced by an Extratropical Cyclone. IEEE Transactions on Geoscience and Remote Sensing, 2016, 54, 7157-7165.	6.3	10
128	Fetch-limited surface wave growth inside tropical cyclones and hurricane wind speed retrieval. , 2016, , .		2
129	Mechanisms for rain effects on Synthetic Aperture Radar. , 2016, , .		2
130	Non-Bragg scattering contributions to the dual-polarized SAR imaging of Hurricane Earl. , 2016, , .		0
131	An automatic method for tropical cyclone center determination from SAR. , 2016, , .		7
132	Coastal zone land-use classification of full-polarization SAR data based on joint sparse. , 2016, , .		0
133	Application of AMSR-E and AMSR2 Low-Frequency Channel Brightness Temperature Data for Hurricane Wind Retrievals. IEEE Transactions on Geoscience and Remote Sensing, 2016, 54, 4501-4512.	6.3	17
134	Extracting hurricane eye morphology from spaceborne SAR images using morphological analysis. ISPRS Journal of Photogrammetry and Remote Sensing, 2016, 117, 115-125.	11.1	38
135	Comparison of Typhoon Centers From SAR and IR Images and Those From Best Track Data Sets. IEEE Transactions on Geoscience and Remote Sensing, 2016, 54, 1000-1012.	6.3	29
136	Preliminary Evaluation of Sentinel-1A Wind Speed Retrievals. IEEE Journal of Selected Topics in Applied Earth Observations and Remote Sensing, 2016, 9, 2638-2642.	4.9	75
137	SAR imaging of mode-2 internal waves in the South China Sea. , 2015, , .		0
138	Synergistic measurements of ocean winds and waves from SAR. Journal of Geophysical Research: Oceans, 2015, 120, 6164-6184.	2.6	29
139	Ocean Wave Parameters Retrieval from TerraSAR-X Images Validated against Buoy Measurements and Model Results. Remote Sensing, 2015, 7, 12815-12828.	4.0	30
140	Early validation of operational SAR wind retrievals from Sentinel-1A. , 2015, , .		0
141	Fetch imaged by SAR and simulated by WRF model. , 2015, , .		1
142	Spot detection from MODIS imagery using 2P-CFAR. , 2015, , .		0
143	NOAA operational SAR winds & amp;#x2014; Current status and plans for Sentinel-1A. , 2015, , .		4
144	A Backscattering Model of Rainfall Over Rough Sea Surface for Synthetic Aperture Radar. IEEE Transactions on Geoscience and Remote Sensing, 2015, 53, 3042-3054.	6.3	59

#	Article	IF	CITATIONS
145	The first Sentinel-1 SAR image of a typhoon. Acta Oceanologica Sinica, 2015, 34, 1-2.	1.0	62
146	SAR imaging of a topography-induced current front in a tidal channel. International Journal of Remote Sensing, 2015, 36, 3563-3574.	2.9	9
147	Remote sensing of spatial-temporal distribution of suspended sediment and analysis of related environmental factors in Hangzhou Bay, China. Remote Sensing Letters, 2015, 6, 597-603.	1.4	27
148	Synergistic Use of Satellite Observations and Numerical Weather Model to Study Atmospheric Occluded Fronts. IEEE Transactions on Geoscience and Remote Sensing, 2015, 53, 5269-5279.	6.3	8
149	Detection of the Hebei Spirit oil spill on SAR imagery and its temporal evolution in a coastal region of the Yellow Sea. Advances in Space Research, 2015, 56, 1079-1093.	2.6	28
150	NOAA/AVHRR sea surface temperature accuracy in the East/Japan Sea. International Journal of Digital Earth, 2015, 8, 784-804.	3.9	20
151	Sea Oil Slick Observation Using Hybrid-Polarity SAR Architecture. IEEE Journal of Oceanic Engineering, 2015, 40, 426-440.	3.8	63
152	Performance Analysis and Validation of Waterline Extraction Approaches Using Single- andÂDual-Polarimetric SAR Data. IEEE Journal of Selected Topics in Applied Earth Observations and Remote Sensing, 2015, , 1-1.	4.9	37
153	Mathematical morphological analysis of typical cyclone eyes on ocean SAR. , 2014, , .		3
154	Oil spill detection in SAR images using multiscale normalized cut segmentation. , 2014, , .		0
155	Inferring internal wave phase speed from multi-satellite observations. , 2014, , .		3
156	Ocean Wind Speed Climatology from Spaceborne SAR Imagery. Bulletin of the American Meteorological Society, 2014, 95, 565-569.	3.3	24
157	Satellite observations of oil spills in Bohai Sea. IOP Conference Series: Earth and Environmental Science, 2014, 17, 012114.	0.3	Ο
158	Observation and simulation of 2010 ULVA prolifera bloom in the Yellow Sea. , 2014, , .		0
159	Coastline detection in SAR images using multiscale normalized cut segmentation. , 2014, , .		11
160	Physics-based scattering model of rainfall over sea surface. , 2014, , .		1
161	Coastline Extraction Using Dual-Polarimetric COSMO-SkyMed PingPong Mode SAR Data. IEEE Geoscience and Remote Sensing Letters, 2014, 11, 104-108.	3.1	66
162	Internal solitary wave propagation observed by tandem satellites. Geophysical Research Letters, 2014, 41, 2077-2085.	4.0	50

#	Article	IF	CITATIONS
163	Tracking the internal waves in the South China Sea with environmental satellite sun glint images. Remote Sensing Letters, 2014, 5, 609-618.	1.4	27
164	Monitoring of Oil Spill Trajectories With COSMO-SkyMed X-Band SAR Images and Model Simulation. IEEE Journal of Selected Topics in Applied Earth Observations and Remote Sensing, 2014, 7, 2895-2901.	4.9	48
165	Summertime sea surface temperature and salinity fronts in the southern Taiwan Strait. International Journal of Remote Sensing, 2014, 35, 4452-4466.	2.9	7
166	Remote sensing of the China Seas. International Journal of Remote Sensing, 2014, 35, 3919-3925.	2.9	4
167	Internal solitary waves in the China seas observed using satellite remote-sensing techniques: a review and perspectives. International Journal of Remote Sensing, 2014, 35, 3926-3946.	2.9	54
168	SAR-derived wind fields at the coastal region in the East/Japan Sea and relation to coastal upwelling. International Journal of Remote Sensing, 2014, 35, 3947-3965.	2.9	28
169	Typhoon eye extraction with an automatic SAR image segmentation method. International Journal of Remote Sensing, 2014, 35, 3978-3993.	2.9	37
170	Shoreline movement monitoring based on SAR images in Shanghai, China. International Journal of Remote Sensing, 2014, 35, 3994-4008.	2.9	22
171	Generation sites of internal solitary waves in the southern Taiwan Strait revealed by MODIS true-colour image observations. International Journal of Remote Sensing, 2014, 35, 4086-4098.	2.9	37
172	SAR monitoring of coastline change in Shanghai, China. IOP Conference Series: Earth and Environmental Science, 2014, 17, 012113.	0.3	0
173	Estimation of tropical cyclone parameters and wind fields from SAR images. Science China Earth Sciences, 2013, 56, 1977-1987.	5.2	33
174	Oil Spill Mapping and Measurement in the Gulf of Mexico With Textural Classifier Neural Network Algorithm (TCNNA). IEEE Journal of Selected Topics in Applied Earth Observations and Remote Sensing, 2013, 6, 2517-2525.	4.9	102
175	Observations of High-Frequency Internal Waves in the Southern Taiwan Strait. Journal of Coastal Research, 2013, 29, 1413.	0.3	22
176	Coexistence of Atmospheric Gravity Waves and Boundary Layer Rolls Observed by SAR*. Journals of the Atmospheric Sciences, 2013, 70, 3448-3459.	1.7	36
177	SAR imaging of ocean surface oil seep trajectories induced by near inertial oscillation. Remote Sensing of Environment, 2013, 130, 182-187.	11.0	34
178	A Systematic Comparison of the Effect of Polarization Ratio Models on Sea Surface Wind Retrieval From C-Band Synthetic Aperture Radar. IEEE Journal of Selected Topics in Applied Earth Observations and Remote Sensing, 2013, 6, 1100-1108.	4.9	59
179	The impact of vertical wind shear on the hurricane eye tilt at the sea and cloud levels. , 2013, , .		2
180	Satellite observations and modeling of oil spill trajectories in the Bohai Sea. Marine Pollution Bulletin, 2013, 71, 107-116.	5.0	80

#	Article	IF	CITATIONS
181	Tropical Cyclone Morphology from Spaceborne Synthetic Aperture Radar. Bulletin of the American Meteorological Society, 2013, 94, 215-230.	3.3	134
182	Fusion of SAR and MODIS images for oceanic internal waves tracking in the South China Sea. , 2013, , .		3
183	Hurricane eye extraction from SAR image using saliency-based visual attention algorithm. , 2013, , .		0
184	Oil platform detection by compact polarimetric synthetic aperture radar. , 2013, , .		2
185	Internal solitary wave refraction at Dongsha Atoll, South China Sea. Geophysical Research Letters, 2013, 40, 3128-3132.	4.0	68
186	Oil-Spill Monitoring in the Coastal Waters of Hong Kong and Vicinity. Marine Geodesy, 2012, 35, 93-106.	2.0	26
187	Ocean surface response to hurricanes observed by SAR. , 2012, , .		2
188	On the role of wind modulation of internal solitary wave signatures in SAR images. , 2012, , .		1
189	Ocean Vector Winds Retrieval From C-Band Fully Polarimetric SAR Measurements. IEEE Transactions on Geoscience and Remote Sensing, 2012, 50, 4252-4261.	6.3	113
190	Validation of SAR-derived sea surface wind products. , 2012, , .		0
191	Polarimetric synthetic aperture radar utilized to track oil spills. Eos, 2012, 93, 161-162.	0.1	33
192	Deepâ€water seamount wakes on SEASAT SAR image in the Gulf Stream region. Geophysical Research Letters, 2012, 39, .	4.0	20
193	ChostNet marine debris survey in the Gulf of Alaska – Satellite guidance and aircraft observations. Marine Pollution Bulletin, 2012, 65, 28-41.	5.0	54
194	Sea surface imprints of coastal mountain lee waves imaged by synthetic aperture radar. Journal of Geophysical Research, 2011, 116, .	3.3	25
195	Mapping sea surface oil slicks using RADARSAT-2 quad-polarization SAR image. Geophysical Research Letters, 2011, 38, n/a-n/a.	4.0	148
196	Monitoring of the water-area variations of Lake Dongting in China with ENVISAT ASAR images. International Journal of Applied Earth Observation and Geoinformation, 2011, 13, 894-901.	2.8	112
197	Ocean Surface Wind Speed of Hurricane Helene Observed by SAR. Procedia Environmental Sciences, 2011, 10, 2097-2101.	1.4	7
198	A Multifrequency Polarimetric SAR Processing Chain to Observe Oil Fields in the Gulf of Mexico. IEEE Transactions on Geoscience and Remote Sensing, 2011, 49, 4729-4737.	6.3	101

#	Article	IF	CITATIONS
199	Comparison of Ocean Surface Winds From ENVISAT ASAR, MetOp ASCAT Scatterometer, Buoy Measurements, and NOGAPS Model. IEEE Transactions on Geoscience and Remote Sensing, 2011, 49, 4743-4750.	6.3	128
200	SAR observation and model tracking of an oil spill event in coastal waters. Marine Pollution Bulletin, 2011, 62, 350-363.	5.0	136
201	Oil spill detection with fully polarimetric UAVSAR data. Marine Pollution Bulletin, 2011, 62, 2611-2618.	5.0	81
202	Comparison of Ocean-Surface Winds Retrieved From QuikSCAT Scatterometer and Radarsat-1 SAR in Offshore Waters of the U.S. West Coast. IEEE Geoscience and Remote Sensing Letters, 2011, 8, 163-167.	3.1	88
203	Ocean sand ridge signatures in the Bohai Sea observed by satellite ocean color and synthetic aperture radar measurements. Remote Sensing of Environment, 2011, 115, 1926-1934.	11.0	36
204	NOAA operational SAR sea surface wind products. , 2011, , .		1
205	The impact of ocean surface features on the high resolution wind retrieval from SAR. , 2011, , .		1
206	SAR observation and WRF simulation of marine atmospheric boundary layer phenomena. , 2011, , .		0
207	Atmospheric frontal gravity waves observed in satellite SAR images of the Bohai Sea and Huanghai Sea. Acta Oceanologica Sinica, 2010, 29, 35-43.	1.0	11
208	Spaceborne sar imaging of coastal ocean phenomena. , 2010, , .		2
209	Deepâ€water bathymetric features imaged by spaceborne SAR in the Gulf Stream region. Geophysical Research Letters, 2010, 37, .	4.0	25
210	Assessment of an analytical model for sea surface wind speed retrieval from spaceborne SAR. International Journal of Remote Sensing, 2010, 31, 993-1008.	2.9	33
211	Identification of ocean oil spills in SAR imagery based on fuzzy logic algorithm. International Journal of Remote Sensing, 2010, 31, 4819-4833.	2.9	57
212	Multisatellite observations and numerical simulation of an alongâ€coast cumulus cloud line induced by seaâ€breeze circulation. International Journal of Remote Sensing, 2009, 30, 3573-3584.	2.9	3
213	Coastal upwelling observed by multi-satellite sensors. Science in China Series D: Earth Sciences, 2009, 52, 1030-1038.	0.9	23
214	Using SAR images to delineate ocean oil slicks with a texture-classifying neural network algorithm (TCNNA). Canadian Journal of Remote Sensing, 2009, 35, 411-421.	2.4	125
215	Sea Surface Manifestation of Along-Tidal-Channel Underwater Ridges Imaged by SAR. IEEE Transactions on Geoscience and Remote Sensing, 2009, 47, 2467-2477.	6.3	47
216	Detection of natural oil slicks in the NW Gulf of Mexico using MODIS imagery. Geophysical Research Letters, 2009, 36, .	4.0	159

#	Article	IF	CITATIONS
217	Circular plumes in Lake Pontchartrain estuary under wind straining. Estuarine, Coastal and Shelf Science, 2008, 80, 161-172.	2.1	47
218	Internal solitary waves in the northwestern South China Sea inferred from satellite images. Geophysical Research Letters, 2008, 35, .	4.0	70
219	High-Velocity Wind Measurements Using Synthetic Aperture Radar. , 2008, , .		2
220	Coastally trapped atmospheric gravity waves on SAR, AVHRR and MODIS images. International Journal of Remote Sensing, 2008, 29, 1621-1634.	2.9	16
221	A SAR Observation and Numerical Study on Ocean Surface Imprints of Atmospheric Vortex Streets. Sensors, 2008, 8, 3321-3334.	3.8	32
222	Ship Detection in SAR Image Based on the Alpha-stable Distribution. Sensors, 2008, 8, 4948-4960.	3.8	77
223	Ship detection algorithm in SAR images based on Alpha-stable model. , 2007, , .		1
224	Coastal katabatic winds imaged by SAR. Geophysical Research Letters, 2007, 34, .	4.0	40
225	Global diagnostics of operational AVHRR SST and aerosol retrievals from NOAA-16 and -17. , 2005, , .		0
226	Synthetic Aperture Radar Imaging of Axial Convergence Fronts in Cook Inlet, Alaska. IEEE Journal of Oceanic Engineering, 2005, 30, 543-551.	3.8	7
227	A cloud line over the Gulf Stream. Geophysical Research Letters, 2004, 31, .	4.0	13
228	Estimating parameters of a two-layer stratified ocean from polarity conversion of internal solitary waves observed in satellite SAR images. Remote Sensing of Environment, 2004, 92, 276-287.	11.0	70
229	Technical note: Evidence of the coexistence of upstream and downstream solitary wavetrains in the real atmosphere. International Journal of Remote Sensing, 2004, 25, 4433-4440.	2.9	7
230	Synthetic aperture radar observation of the sea surface imprints of upstream atmospheric solitons generated by flow impeded by an island. Journal of Geophysical Research, 2004, 109, .	3.3	37
231	Analyzing the dependence between RADARSAT-1 vessel detection and vessel heading using CFAR algorithm for use on fishery management. , 2003, , .		1
232	A two-scale model to predict C-band VV and HH normalized radar cross section values over the ocean. Canadian Journal of Remote Sensing, 2002, 28, 367-384.	2.4	47
233	An extraordinary breach of the Gulf Stream north wall by a cold water intrusion. Geophysical Research Letters, 2002, 29, 8-1-8-4.	4.0	4
234	Observation of hurricane-generated ocean swell refraction at the Gulf Stream north wall with the RADARSAT-1 synthetic aperture radar. IEEE Transactions on Geoscience and Remote Sensing, 2002, 40, 2131-2142.	6.3	61

#	Article	IF	CITATIONS
235	Analysis of coastal lee waves along the coast of Texas observed in advanced very high resolution radiometer images. Journal of Geophysical Research, 2001, 106, 7017-7025.	3.3	18
236	Validation of coastal sea and lake surface temperature measurements derived from NOAA/AVHRR data. International Journal of Remote Sensing, 2001, 22, 1285-1303.	2.9	93
237	Analysis and Modeling of Atmospheric Gravity Waves Observed in RADARSAT SAR Images. Remote Sensing of Environment, 2000, 74, 343-361.	11.0	43
238	Atmospheric vortex streets on a RADARSAT SAR image. Geophysical Research Letters, 2000, 27, 1655-1658.	4.0	44
239	Routine Monitoring of Changes in the Columbia Glacier, Alaska, with Synthetic Aperture Radar. Remote Sensing of Environment, 1999, 70, 257-264.	11.0	5
240	The Use of Pre-Storm Boundary-Layer Baroclinicity in Determining and Operationally Implementing the Atlantic Surface Cyclone Intensification Index. Boundary-Layer Meteorology, 1998, 89, 211-224.	2.3	3
241	Evidence and mechanism of Hurricane Fran-Induced ocean cooling in the Charleston Trough. Geophysical Research Letters, 1998, 25, 769-772.	4.0	12
242	Mesoscale oceanic and atmospheric feature detection through fusion of RADARSAT SAR with GOES/Imager data. , 1998, , .		1
243	The sea surface imprint of island lee waves as observed by RADARSAT synthetic aperture radar. , 1998, , .		3
244	Analysis of atmospheric vortex streets observed on SAR image. , 0, , .		0
245	Analysis of ocean surface features with coincident SAR and radiometer data within the Alaska SAR Demonstration. , 0, , .		2
246	Validation of an automatic vessel detection algorithm using SAR data and known vessel fleet distributions. , 0, , .		6
247	Validation of a CFAR vessel detection algorithm using known vessel locations. , 0, , .		12
248	NOAA CoastWatch RADARSAT-1 SAR coastal monitoring applications demonstrations. , 0, , .		1
249	SAR and MODIS images of atmospheric solitary waves generated by upstream blocking in flow over St. Lawrence Island Bering Sea. , 0, , .		0
250	SAR-derived winds in Coastal Alaska waters. , 0, , .		0
251	Eddy detection using RADARSAT-1 synthetic aperture radar. , 0, , .		2
252	Analysis of island wakes and katabatic winds imaged by RADARSAT-1 synthetic aperture radar. , 0, , .		0

#	Article	IF	CITATIONS
253	Analysis of oceanic long wave refraction at the Gulf Stream boundary using RADARSAT synthetic aperture radar during Hurricane Bonnie. , 0, , .		1